

# Limits of complete equilibration of fragments produced in central Au on Au collisions at intermediate energies

W. Neubert<sup>1</sup> and A.S.Botvina<sup>2,3</sup>

<sup>1</sup> Institut für Kern- und Hadronenphysik, Forschungszentrum Rossendorf, 01314 Dresden, Germany

<sup>2</sup> Gesellschaft für Schwerionenforschung, 64291 Darmstadt, Germany

<sup>3</sup> Institute for Nuclear Research, Russian Academy of Science, 117312 Moscow, Russia

Received: November 20, 2018

**Abstract.** Experimental data related to fragment production in central Au on Au collisions were analysed in the framework of a modified statistical model which considers cluster production both prior and at the equilibrated stage. The analysis provides limits to the number of nucleons and to the temperature of the equilibrated source. The rather moderate temperatures obtained from experimental double-yield ratios of  $d,t$ ,  ${}^3\text{He}$  and  ${}^4\text{He}$  are in agreement with the model calculations. A phenomenological relation was established between the collective flow and the chemical temperature in these reactions. It is shown that dynamical mechanisms of fragment production, e.g. coalescence, dominate at high energies. It is demonstrated that coalescence may be consistent with chemical equilibrium between the produced fragments. The different meaning of chemical and kinetic temperatures is discussed.

**PACS.** 25.70.Mn , 25.70 Pq , 25.75.-q

## 1 Introduction

The mechanism of fragment production at intermediate energy nucleus-nucleus collisions is a long standing problem which is important for many investigations, such as the study of the nuclear liquid-gas phase transition, the behaviour of nuclear matter under extreme conditions, and, in general, the nuclear equation of state. In this paper we concentrate on central collisions which deposit a large amount of energy into nuclei, and produce a fast explosion of nuclei into many fragments. Presently, there is evidence that at low projectile energies of  $\sim 10$ – $100$  A·MeV the fragment production via multifragmentation of thermal-like sources is the dominating process [1,2,3,4]. With increasing energy dynamical effects, such as collective flow, becomes prominent. This implies that the fragmentation mechanism changes from a statistical to a dynamical one. However, the description of intermediate mass fragment (IMF) production as a result of the break-up of an equilibrated source with collective flow is very successful, as shown in many publications [3,5,6]. We believe that such good descriptions were possible since the hypothesis of chemical equilibrium between different kinds of fragments is adequate for these reactions.

In this paper we analyse data from 100 to 1000 A·MeV. Some of these data were already analysed with different dynamical and statistical approaches. The present analysis involves new degrees of freedom. In particular, it emphasizes the importance of isospin characteristics of pro-

duced fragments for the determination of the reaction mechanism.

As suggested by many theoretical and experimental studies [3,5,7,8,9,10,11] the fragments may be produced in a fast initial ('preequilibrium') process as well as at the full equilibration stage. Since the number of nucleons participating in the thermal-like source can decrease rapidly with the beam energy, dynamical processes of fragment formation should contribute essentially at higher energies. The mechanism of coalescence of nucleons into fragments is applied here for a complementary description of light fragment production to the statistical approach. In the following we discuss a relation between coalescence and statistical approaches and we point out that the coalescence mechanism may simulate the chemical equilibrium conditions. In this respect, we pay special attention to the chemical temperature and study its correlation with the light charged particles (LCP) velocities. However, our main aim is to determine properties of a completely equilibrated source, which is mainly responsible for IMF production. We emphasize, that the conclusions about equilibrium and nonequilibrium contributions concerns the production of fragments from nucleons only. We do not consider the problem of the nucleon thermalization and refer to experimentally selected central events which belong to an ensemble of nucleons in some degree of equilibration. The knowledge of the relation between equilibrium and non-equilibrium mechanisms of fragment production in dynamical processes is important for many

applications both in nuclear physics and astrophysics. For example, similar processes are expected during the fast synthesis of elements in the early universe and in supernova explosions [12].

## 2 Chemical temperatures evaluated from fragment data obtained in central Au+Au collisions

Data obtained by the FOPI collaboration at 100, 150, 250 and 400 A·MeV [13,15] and data from the EOS collaboration [16,17,18] at 1 A·GeV are analysed. Central events were selected by the criterion ERAT as described in ref. [13] whereas the event centrality of the 1 A·GeV data was determined by multiplicity cuts (see ref. [17]).

It is commonly accepted that the kinetic energies of fragments can be represented as a sum of thermal and collective components. The collective motion (radial flow) is an important ingredient of Au on Au collisions at intermediate energies and influences strongly the fragment energies. Kinetic energy distributions for central events have been analysed in the framework of the 'blast model' which is described in detail in ref. [13]. Here, we recall briefly only the main aspects. The collective energy stored into radial flow was determined by velocity profiles and an ansatz for the velocity distribution [19] of the fragments. The corresponding kinetic energy distributions were reproduced if the collective energy  $\varepsilon_{coll}$  amounts to  $62 \pm 8$  % of the center-of-mass energy  $E_{C.M.}$  available in the collision. Then, the energy conservation requires that

$$\varepsilon_{coll} + \varepsilon_{th} = E_{C.M.} + Q \quad (1)$$

where  $Q$  is the Q-value of the reaction and  $\varepsilon_{th}$  is the thermal energy. In the limit of classical statistics the temperature is determined by the multiplicities  $N$  of the emitted particles using the non-relativistic expression

$$\varepsilon_{th} = \frac{3}{2} \cdot (N - 1) \cdot T^*. \quad (2)$$

The temperatures found by this approach are  $T^* = 17.2 \pm 3.4$ ,  $26.2 \pm 5.1$  and  $36.7 \pm 7.5$  MeV for the beam energies 150, 250 and 400 A·MeV, respectively. Below we label them as 'kinetic' temperatures  $T_{kin}$ . It was emphasized that the temperatures  $T^*$  are 'effective' in the sense that they are not the temperature at freeze-out time, since the observed multiplicity may be raised due to late particle decays. In ref.[13], these temperatures were used as input for the statistical multifragmentation models QSM [20], WIX [21] and SMM [22] by assuming that the whole entire mass of the colliding Au nuclei undergoes thermalization. This assumption fails to reproduce the fragment multiplicities. The abundances of heavy clusters are underestimated up to 4 orders of magnitude (e.g. for  $Z=8$  fragments at 400 A·MeV.) In ref.[13] it was discussed that variations of the radial flow energy, the freeze-out densities and level density parameters within reasonable physical limits cannot account for such large deviations. Hence,

the question arises about the applicability of established statistical models to cluster production in the midrapidity source and the meaning of the nuclear temperatures mentioned above. The present paper is intended to help to disentangle this 'puzzle'. First we ask whether these temperatures can be confirmed by other data available for the same collision system Au+Au measured with the same apparatus. Such possibility offer the yields of hydrogen and helium isotopes [15] which can be treated by the isotope thermometry.

In ref. [23] it was shown that in an equilibrated system the double-yield ratio ( $R_1/R_2$ ) of isotopes is directly related to the temperature of the corresponding grand canonical ensemble:

$$T_{iso} = \frac{b}{\ln(a \cdot (R_1/R_2))}. \quad (3)$$

For the consideration of hydrogen ( $d, t$ ) and helium isotopes ( ${}^3He, {}^4He$ ) one needs to fix the parameters  $b=14.32$  MeV and  $a=1.59$  [24] which include the binding energies, masses and spin degeneracy. This isotope thermometer has proved to be successful in many applications. In particular, for the first time it was possible to establish experimentally the nuclear caloric curve [25].

Here, we refer to the isotopic yield ratios and kinetic energy distributions of  $d$ ,  $t$ ,  ${}^3He$  and  ${}^4He$  measured with  $\Delta E/E$  telescopes within the C.M. polar angle range of  $60^\circ \leq \Theta_{C.M.} \leq 90^\circ$  [15]. Most of the projectile fragments are expected to be suppressed within this angular coverage. The corresponding data sets at 100, 150 and 250 A·MeV were obtained from central event samples selected by the criterion ERAT5 [13]. The integration of the C.M.-kinetic energy spectra delivered the intensity of deuterons, tritons,  ${}^3He$  and  ${}^4He$  from which the ratios  $R_1$  and  $R_2$  and the corresponding isotope temperature  $T_{iso}$  were determined. The obtained values  $\langle T_{iso} \rangle = 6.34 \pm 0.50$ ,  $7.8 \pm 0.8$  and  $11.51 \pm 1.58$  MeV for 100, 150 and 250 A·MeV, respectively, are about three times smaller than the corresponding kinetic temperatures. More details of the distribution of  $T_{iso}$  in the freeze-out volume are required. Here, we determined from the LCP spectra presented in ref. [15] the isotope temperature in dependence on the velocity.

The C.M. kinetic energies  $E_{kin}$  were transformed into the particle C.M. velocities using the relativistic relation

$$\frac{v}{c} = \frac{\sqrt{E_{kin}(E_{kin} + 2mc^2)}}{E_{kin} + mc^2} \quad (4)$$

where  $m$  is the corresponding LCP mass,  $c$  is the light velocity. The spectra given in ref. [15] have an equidistant energy binning for all particles. But, the velocity divisions become varying for different particle masses after the abscissa transformation. In order to cover the same range of velocities we analysed the kinetic energy distributions to  $E_{kin}(d) < 110$  MeV,  $E_{kin}(t, {}^3He) < 150$  MeV and  $E_{kin}({}^4He) < 200$  MeV for incident energies 100 and 150 A·MeV. The corresponding limits are 170, 250 and 300 MeV at 250 A·MeV. Equal reference velocities  $v_i$  for the four LCP's were found by an appropriate interpolation

of the velocity distributions derived within these limits. The maximum velocity up to which yields of all LCP's were available was around  $0.3\cdot c$  at 250 A·MeV and  $0.6\cdot c$  at 1 A·GeV, respectively. Then, the isotope temperature  $T_{iso}$  was recalculated for subsequent velocities  $v_i$  by means of equation (3) with the ratios

$$\begin{aligned} R_1 &= Y(d, v_i)/Y(t, v_i) \\ R_2 &= Y(^3He, v_i)/Y(^4He, v_i). \end{aligned} \quad (5)$$

The mean temperatures evaluated within the limited velocity ranges are  $\langle T_{iso} \rangle = 5.30, 6.10$  and  $9.14 \pm 0.60$  MeV, respectively, for 100, 150 and 250 A·MeV. They are smaller than the values derived from the yields integrated over the complete energy spectrum, since the contributions of fragments with the highest energies are missing. However, this treatment is self-consistent for this subset of events, where the collective flow dominates over Coulomb and thermal energies and determines mostly the fragment velocities.

As shown in Fig. 1 the temperatures  $T_{iso}$  become larger with increasing particle velocity, however, they are below the kinetic temperatures  $T^*$  of ref. [13]. This finding suggests that the obtained data cannot be described by *one* temperature characterizing the complete equilibrium. An explanation of this phenomenon could be that fast (preequilibrium) nucleons are emitted earlier at very high temperatures and carry away excess energy, while slow nucleons form an equilibrium-like source [7]. The observed light fragments are produced during the cooling process and the distribution of the chemical temperature versus the fragment velocity reflects evolution toward equilibrium. Figure 1 shows that in all cases the temperature  $T_{iso}$  has some saturation at low velocities. This could be an evidence for reaching thermalization of nuclear matter at these velocities. Obviously, this thermal source can be characterized by very moderate *chemical* temperatures.

It is a general observation (e.g., see [11]) that in intermediate energy collisions the kinetic energy spectra of fragments cannot be reproduced by using an unique temperature. In the following we propose a model to describe these feature.

### 3 Description of the model

An appropriate way to describe processes involving many particles is the statistical approach. The system characterized in the initial stage by nonequilibrium distribution functions evolves towards equilibration as a result of many interactions between the particles. In this process the system runs through different states. The first one can be considered as equilibration of the one-particle degrees of freedom. The following evolution toward total thermalization can be considered as involving of higher order particle correlations. For finite expanding systems the degree of equilibration depends on the reaction type. It is expected that the equilibration is less effective for nucleons at the surface than for nucleons deep inside the freeze-out volume. As a result, the mechanisms of the fragment production may be different also.

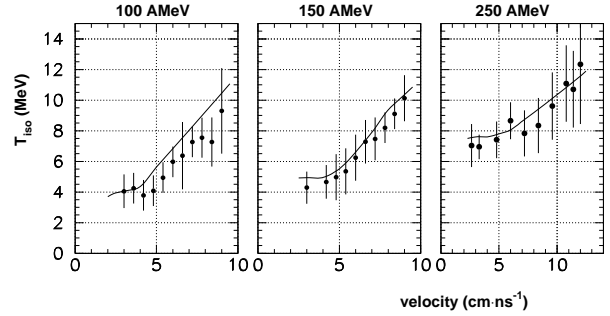


**Fig. 1.** Isotopic temperatures evaluated from the data in ref. [15] as a function of the C.M. velocities of  $d, t, ^3He$  and  $^4He$ . Dots: data. Lines: calculations with the code SMMFC including contributions from the fast stage (coalescence).

In the following we are going to interpret the experimental data within the framework of the expanded version of the statistical multifragmentation model [1,22] which treats also LCP's emitted prior to the equilibration. The model phenomenologically includes collective motion (radial flow ( $F$ )) and, optionally, composite particle production by a new coalescence ( $C$ ) algorithm.<sup>1</sup> The subsequent application of these mechanisms is aimed at simulating the most important physical processes in many-particle systems.

The model parameters have to be derived from fits to the experimental data as described in section 4. It is important to use as many as possible observables for the analysis, and to ensure that the deduced parameters and their dependence on the beam energy are qualitatively consistent with general predictions of dynamical calculations [7].

Total energy and momentum balance is used for the implemented processes (except  $\gamma$ -emission). First we consider the quantities being constrained. A projectile with mass number  $A_1$  and charge  $Z_1$  collides at beam energy  $E_{beam}$  with a target ( $A_2, Z_2$ ) resulting in the center-of-mass energy  $E_{C.M.}$  available for the total system with  $A_0 = A_1 + A_2$  and  $Z_0 = Z_1 + Z_2$ . Since the equilibrated stage is rather well understood, we start the analysis of experimental data related to IMF's which are assumed to be produced only in the equilibrated (i.e. thermal) source. This source is parametrized by (i) the mass number  $A_s = A_{rel} \cdot A_0$  (where  $A_{rel}$  is the relative source size) and corresponding charge  $Z_s = A_s \cdot (Z_0/A_0)$ , (ii) the thermal excitation energy  $E^*$  and (iii) the collective energy per nucleon  $E_{flow}$ . In the analysis of the 1 A·GeV data the energy released due to pion production was taken into account.  $P_\pi$  is the part of  $E_{C.M.}$  taken away by pions. The remaining matter ( $A_{pre} = A_0 - A_s, Z_{pre} = Z_0 - Z_s$ ) is assumed to be carried away by fast nucleons and LCP preequilibrium emission. In this case the change of the binding energy is given by the corresponding values for projec-

<sup>1</sup> henceforth the sign SMMFC denotes this code version

tile, target, thermal and preequilibrium sources:  $\Delta B = B_1 + B_2 - B_s - B_{pre}$ . From the conservation of the total energy follows the energy available for preequilibrium emission:  $E_{pre} = E_{C.M.} - P_\pi \cdot E_{C.M.} - E^* - E_{flow} + \Delta B$ .

### 3.1 LCP emission at the fast stage.

Since the cooling during the expansion process is very fast, nucleons have no time to feel the part of the phase space corresponding to the composite particle production. A distribution of nucleons in the phase space at some 'freeze-out' time is considered as start configuration. Generally, any distribution of nucleons in momentum and coordinate space after an initial dynamical process is conceivable. But, in some experiments, e.g. central nucleus–nucleus collisions [13], it is possible to select samples which are nearly isotropic in space and look like thermal events. Therefore, in such cases, we can simply assume that the nucleons populate the available *many-body* phase space uniformly, i.e. there is equilibration in one-particle degrees of freedom without manifestation of collective phenomena. That gives rise to a thermal distribution for individual nucleons in the thermodynamical limit. In the calculations we consider the system characterized by  $A_{pre}$ ,  $Z_{pre}$  and  $E_{pre}$  and disintegrate the system into nucleons by taking away about 7 A·MeV (binding energy). The remaining energy turns into the kinetic energies of nucleons which populate the whole available many-body momentum space uniformly. The procedure developed in [26] is used to generate the nucleon momenta.

A composite particle can be formed from two or more nucleons if they are close to each other in the phase space. This simple prescription is known as coalescence model. Here we use the coalescence in momentum space which was recently described and applied in ref. [29]. The basic assumption is that a dynamical process, which leads to a momentum redistribution, is very fast (nearly instantaneous), so that the coordinates of nucleons are just defined by their momenta. This is also justified taking into account quantum properties of the system since the wave functions of nucleons can be described in momentum space only. This type of coalescence model has proven successfully by reproducing experimental data (see e.g. [30,31,32]).

In the standard formulation of the model it is assumed that the fragment density in momentum space is proportional to the momentum density of nucleons times the probability of finding nucleons within a small sphere of the coalescence radius  $p_0$ . For example, in a nonrelativistic approximation, from this hypothesis an analytical expression can be derived for momentum spectra of coalescent clusters:

$$\frac{d^3 \langle N_A \rangle}{d\bar{p}_n^3} \simeq \left( \frac{4\pi}{3} p_0^3 \right)^{A-1} \left( \frac{d^3 \langle N_1 \rangle}{d^3 \bar{p}_n} \right)^A \quad (6)$$

where  $\bar{p}_n$  are the momenta per nucleon.  $\langle N_A \rangle$  and  $\langle N_1 \rangle$  are the mean multiplicities of fragments with the mass

numbers  $A$  and 1, respectively. This equation disregards correlations between different clusters since the conservation of the nucleon number is not taken into account. Therefore, the above formulae is valid only for  $\langle N_1 \rangle \gg \langle N_2 \rangle \gg \langle N_3 \rangle \dots$

We developed another formulation of the coalescence model. Nucleons can produce a cluster with mass number  $A$  if their momenta relative to the center-of-mass moment of the cluster is less than  $p_0$ . Accordingly we take  $|\mathbf{p}_i - \mathbf{p}_{C.M.}| < p_0$  for all  $i = 1, \dots, A$ , where  $\mathbf{p}_{C.M.} = \frac{1}{A} \sum_{i=1}^A \mathbf{p}_i$ . In the following examples the value  $p_0 \approx 94 \text{ MeV}/c$  has been adopted corresponding to relative velocities  $v_{rel} = 0.1c$  in agreement with previous analyses [29].

In this context we would like to draw attention to a problem which is sometimes disregarded in these simulations. Some nucleons may have such momenta that they can belong to different coalescent clusters according to the coalescence criterion. In these cases the final decision depends on the sequence of nucleons within the algorithm. To avoid this uncertainty we developed an iterative coalescence procedure.  $\mathcal{M}$  steps are calculated in the coalescence routine with the radius  $p_{0j}$  which is increased at each step  $j$ :  $p_{0j} = (j/\mathcal{M}) \cdot p_0$  ( $j = 1, \dots, \mathcal{M}$ ). Clusters produced at earlier steps participate as a whole in the following steps. In this case the final clusters not only meet the coalescence criterion but also the nucleons have the minimum distance in the momentum space. This procedure is unique in the limit  $\mathcal{M} \rightarrow \infty$  and we found that in practical calculations it is sufficient to use  $\mathcal{M} = 5$ .

The importance of this coalescence mechanism is demonstrated by Fig. 2 which shows a comparison of measured isotopic yield ratios  $d/t$  and  ${}^3\text{He}/{}^4\text{He}$  in the beam energy range from 35 A·MeV to 1 A·GeV [15,16,27,28]. Especially at higher incident energies the SMM calculations without consideration of coalescence underestimate strongly the existing data. The so-called ' ${}^3\text{He} - {}^4\text{He}$  puzzle' can also be solved by taking into account the coalescence [29].

In the calculations we assume that only coalescent particles with  $A \leq 4$  are produced. In principle, one can extend the model by considering IMF also, though the probabilities of coalescent IMF is small [32,29]. In this case the expected portion of the thermal source will be even smaller than with restriction to  $A \leq 4$ . However, this paper is aimed at finding an upper limit for the contribution of thermal IMF's. As justification of our assumption we present a good agreement with experimental data in section 5. There are also other experimental features supporting this assumption. In particular, the maximum of IMF production was found at small fragment velocities. These velocities correspond to the nearly constant temperatures  $T_{iso}$  (see Fig. 1) associated with a thermal-like source.

### 3.2 Thermal source

At the freeze-out time of several tens of fm/c there is still a lot of relative dense nuclear matter in the center of the system in which instabilities (usually associated with the

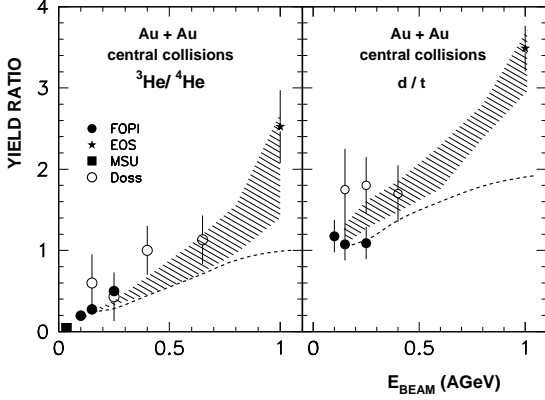


**Fig. 2.** Isotopic yield ratios of LCP in central Au on Au collisions as a function of the beam energy. Data are displayed by symbols: FOPI [15], EOS [16], MSU [27], Doss [28]. The hatched areas show SMMFC calculations assuming the uncertainty of the input parameters given in table 1. Dashed lines: Calculations using only the thermal source (without coalescence) and the same input (without consideration of uncertainty limits).

liquid-gas type transition) may occur. At this stage it is assumed that *thermal equilibrium* is reached, which is responsible for IMF production. The success of the SMM and other statistical models [1, 21, 33] to describe such reactions (see e.g. refs. [1, 2, 3, 4, 5, 6]) supports this assumption.

A microcanonical ensemble of all break-up partitions which consist of nucleons and excited fragments of different masses [1] is considered. If  $E^*$  and the volume of the thermal source are fixed, the statistical weight  $W$  of a given break-up partition  $j$  (i.e. the number of microscopic states leading to this partition) is determined by its entropy  $S_j$ :

$$W_j^{mic} \propto \exp(S_j(E^*, A_s, Z_s)). \quad (7)$$

The fragments with mass number  $A > 4$  are treated as heated nuclear liquid drops but the light fragments with  $A \leq 4$  are considered as massive particles ('nuclear gas') having only translational degrees of freedom. The ensemble of partitions is generated by Monte-Carlo methods according to their statistical weights  $W_j$  constrained by the conservation laws. The microcanonical temperature  $T_{th}$  is found from the energy balance by taking into account the Coulomb interaction, binding energies and excitations of fragments. After break-up of the system the fragments propagate independently in their mutual Coulomb fields and undergo secondary decays. The deexcitation of large fragments ( $A > 16$ ) is described by the evaporation-fission model, and for smaller fragments by the Fermi break-up model [22, 34].

### 3.3 Relation between coalescence mechanism and thermal fragment production.

An important relationship can be formally established between the coalescence and thermal models as far as fragment production is considered. This will be illustrated by a simple statistical case. A system with the total number of nucleons  $A_0$  disintegrates into fragments with mass number  $A$ , which are characterized only by their binding energy  $B_A$ . The fragments are considered as Boltzmann particles moving without interaction in the volume  $V$ . Then the statistical partition sum can be calculated as

$$\eta = \sum_{partitions} \left( \prod_A \frac{V}{(2\pi\hbar)^3} \int d^3\bar{p} \cdot e^{-\frac{\bar{p}^2}{2m_n A T}} \cdot P_A \right), \quad (8)$$

where  $T$  is the kinetic temperature characterizing the fragment translational motion,  $m_n \approx 0.94$  GeV is the nucleon mass and  $\bar{p}$  is the fragment momentum. The product includes all fragments in a partition. The momentum and the center of mass conservations are disregarded. The magnitude  $P_A$  is proportional to the probability of the formation of fragment  $A$ , which can be written as  $P_A = \exp(-B_A/T)$  in the case of full equilibration characterized by the canonical temperature  $T$ . However, the process of fragment formation may be complicated, and this process may not be related only to the thermal kinetic motion. Generally, one can write  $P_A = \exp(-B_A/T_A)$ , where  $T_A$  is a parameter ('temperature') related to a given fragment. One can introduce a Lagrange multiplier  $\mu$  (like a 'chemical potential'), which can be found from the condition  $\sum_A \langle N_A \rangle A = A_0$  (see ref. [1]). Then the partition sum can be calculated as

$$\eta = \sum_{N_1=0}^{\infty} \cdots \sum_{N_{A_0}=0}^{\infty} \prod_A \left[ \frac{\langle N_A \rangle^{N_A}}{N_A!} \right]. \quad (9)$$

Here  $N_A$  is the multiplicity of fragment  $A$  in a partition, and

$$\langle N_A \rangle = \frac{V}{\lambda_T^3} A^{3/2} \exp \left[ -\frac{B_A}{T_A} + \mu A \right], \quad (10)$$

with the thermal wavelength  $\lambda_T = (2\pi\hbar^2/m_n T)^{1/2}$ . The last equation can be rewritten as

$$\langle N_A \rangle = \langle N_1 \rangle^A \left( \frac{\lambda_T^3}{V} \right)^{A-1} A^{3/2} \exp \left( -\frac{B_A}{T_A} \right). \quad (11)$$

At this point we can establish a correspondence between the thermal and the coalescence models (see also [35]). In the coalescence model, the fragment multiplicity can be determined after integration of equation (6). If the nucleons are assumed to have a Maxwell-Boltzmann distribution of the same kinetic temperature one can easily get

$$\langle N_A \rangle \simeq \left( \frac{4\pi}{3} p_0^3 \right)^{A-1} \frac{\langle N_1 \rangle^A}{(2\pi m_n T)^{3/2(A-1)} A^{3/2}}. \quad (12)$$

By comparing equations (12) and (11) we obtain a formal relation between the model parameters:

$$\frac{4\pi p_0^3 V}{3h^3} \simeq \left( A^3 \cdot \exp\left(-\frac{B_A}{T_A}\right) \right)^{1/(A-1)}. \quad (13)$$

A possible physical interpretation of this relation is the following. If we assume that the freeze-out density and the coalescence parameter are determined by a short range interaction between nucleons and properties of formed fragments, then there is an effective 'temperature'  $T_A$  which characterizes the produced coalescent fragments. In the case of saturation of the binding energy, i.e.  $B_A \sim A$ , the effective temperatures do not differ much for fragments with different  $A$ . That resembles the chemical temperature, when the relative probabilities of different fragments are determined by this temperature. One can see that the isotope temperature defined by equation (3) corresponds exactly to this temperature. Moreover, one can also use relation (13) in another way, namely, one can determine the coalescence parameters  $p_0$  for different fragments from the experimentally obtained chemical temperatures [36]. Therefore, if statistical models are applied to interpret processes with strong dynamical features, we should take into account that the fragment velocities may be determined by the kinetic temperature (or by the initial dynamics) but not by the chemical temperature.

### 3.4 Radial flow

After a central collision the collective expansion is assumed to change only the velocity of the fragments taken into account by a flow velocity profile  $\mathbf{v}_f(r) = (\mathbf{r}/R) \cdot v_0$  proportional to the position  $\mathbf{r}$  from the center of the disassembling equilibrated source [1]. Within this scenario the flow velocity is superimposed onto the stochastic motion of the generated fragments and only the stochastic thermal part is responsible for fragment production. The radial flow is supposed to change the fragment velocities but not the fragment yields. This ansatz comes from the hydrodynamical picture, however, in the case of nuclear multifragmentation there are theoretical arguments for using this approach at  $E_{flow} \leq 3$  A·MeV [1,37]. In this paper we extend it also to higher flow energies in order to find limits of this approach by analyzing the experimental data. The adequacy of the above ansatz is formally supported by statistical-like properties of fragments produced in a dynamical process such as coalescence. The lattice model calculations [38] show also that the flow may not influence statistical fragment formation.

This hypothesis of decoupling thermal and collective motions is sufficient for a reasonable reproduction of experimental data [3,4,5,6]. By introducing the phenomenological radial flow profile we fit the IMF velocities, however, we do not explain the velocities. Nevertheless, since we conserve the total energy and momentum in the system, this receipt allows to simulate individual multifragmentation events and to compare them directly with experimental data.

The described modified statistical model does not pretend to be a complete substitute for dynamical calculations but it should be considered as a effective tool for a primary analysis of experimental data. Then, the observables being properly reproduced, the physical meaning of the fitted parameters can be interpreted. The knowledge of these parameters (in particular, the temperatures) is supposed to be important for applications of thermal descriptions for many nuclear processes. The code SMMFC allows us to perform calculations with high statistics for large systems, as Au on Au, with reasonable computing time. The code produces event distributions directly related to the observables, e.g. the multiplicity of an event as well as the charge, the mass, the kinetic energy and the polar and azimuthal angles. In this way, the generation of single events allow us to process the calculated quantities in a way like the experimental data samples. Our implemented filter permits to study the influence of the detector geometry and resolution, the Z-dependent registration thresholds and chosen cut conditions.

## 4 Adjustment of the model parameters

The following four parameters of the model (see section 3)

$$E^*, A_{rel}, E_{flow} \text{ and } P_\pi$$

determine the fragment production. The influence of the break-up density  $\varrho$  is discussed below. A scanning over the complete parameter space, used in [7,8], is too time-consuming in our case so that we disentangle this coupled parameter set by finding specific sensitivities of the parameters to certain observables. We refer in the following only to the key observables which are necessary to fix the model parameters.

### 4.1 Thermal excitation energy

Multiplicity distributions of charged particles from central Au+Au collisions (ref. [13]) are plotted in Fig. 3. In addition, our results obtained from a subset of data selected by the centrality criterion  $ERAT \geq 0.7$  and  $\Theta_{C.M.} \geq 25^\circ$  are also shown in this figure. Since the experimental distributions have a nearly exponential shape  $dN/dZ \propto \exp(-\alpha Z)$  over the whole range of measured charges, they can be fit by an exponential form. We included into the fits only the part of the charge distributions with  $Z \geq 3$  to exclude the influence of LCP on the parameter  $\alpha$ . In ref. [13] also the  $Z=4$  points were excluded from the fits performed within  $3 \leq Z \leq 10$ . Our fit parameters  $\alpha(3 \leq Z \leq 6)$  obtained from the mentioned subset are somewhat larger than the corresponding one's of ref. [13]. Since the errors  $\Delta\alpha$  from each fit are small compared to possible disturbance of the charge distribution by evaporative processes and sequential decays, we used the difference between the fit values given in ref. [13] and  $\alpha(3 \leq Z \leq 6)$  as a measure of possible deviations.

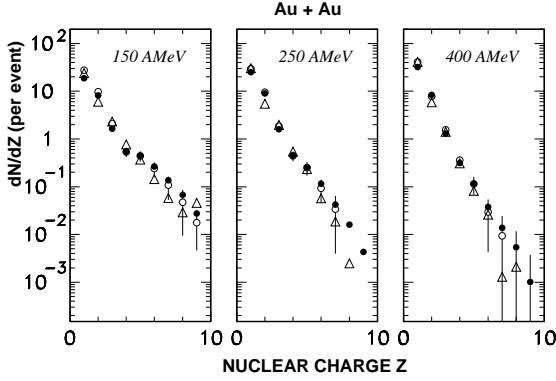


**Fig. 3.** Measured and simulated multiplicities  $N$  of nuclear charges. Black dots: data from ref. [13]. Open triangles: subset of data analysed by the selection criterion  $ERAT \geq 0.7$  and  $\Theta_{C.M.} \geq 25^\circ$  within the plastic wall acceptance, Open circles: filtered model calculations with input parameters from table 1. The calculated  $Z=1,2$  multiplicities contain contents from both the preequilibrium and thermalized sources.

The parameters  $\alpha$  derived from the data are nearly proportional to the available center-of-mass energy. Otherwords, the calculated charge distributions show that the steepness parameter  $\alpha$  ( $3 \leq Z \leq 6$ ) increases also linearly with the excitation energy of the thermal source. In order to find a quantitative relation, numerous charge distributions were simulated at various excitation energies. From a linear fit within the limits  $3 \leq Z \leq 6$  we found the relation  $\alpha = -0.571 + 0.1508 \cdot E^*$  within the considered ranges of the source parameters. This result is nearly independent on the source size  $A_{rel}$ , freeze-out density  $\rho$  and the radial flow  $E_{flow}$ . Steepness parameters  $\alpha$  obtained from calculated charge yields for the full phase space deviate only by a few percents from those which were processed by the filter routine implemented in SMMFC.

The procedure of determining the parameters at 250 A·MeV is illustrated in Fig. 4. The values  $\alpha=0.91$  and  $\alpha=1.15$  [13] found from fits to the data determine the interval of the corresponding excitation energy  $E^*$  (upper panel of Fig. 4).

#### 4.2 Size of the thermal source

The interval of excitation energies being fixed, we are going to estimate the relative source size  $A_{rel}$  by means of the IMF multiplicity which depends in terms of SMMFC on both  $A_{rel}$  and  $E^*$ . The lower panel of Fig. 4. demonstrates how  $A_{rel}$  is estimated from the overlap of the experimental IMF multiplicity [13] with the calculated one's.  $A_{rel} = 0.50 \pm 0.05$  at 250 A·MeV is consistent with both the multiplicity data and the estimated limits of  $E^*$ . The expected sizes of the equilibrated source at 150 A·MeV and 400 A·MeV have been obtained analogously and the results are given in table 1. These parameters are consistent with those extracted in ref. [3] at somewhat lower incident energies. The obtained trend of the decreasing

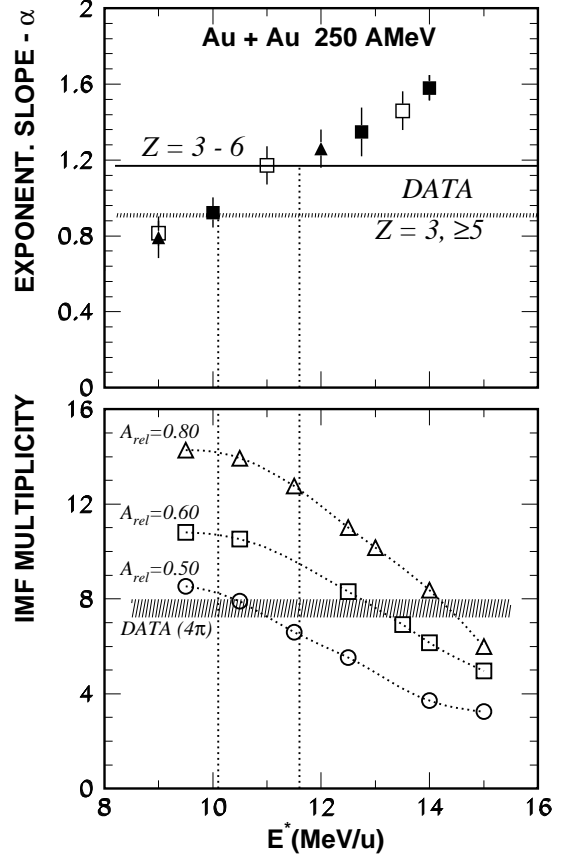


**Fig. 4.** Determination of the input parameters of the model. Upper part: steepness parameter  $\alpha$  vs. excitation energy  $E^*$ . Dashed horizontal lines: data taken from [13] and this work. SMMFC calculations are denoted by symbols. Full squares:  $E_{flow} = 0.55 \cdot E_{C.M.}$ ,  $A_{rel} = 0.5$ , Open squares:  $E_{flow} = 0.37 \cdot E_{C.M.}$ ,  $A_{rel} = 0.3$ . Lower part: IMF multiplicity ( $3 \leq Z \leq 6$ ) vs. excitation energy. Hatched area: data from ref.[13]. The symbols are SMMFC calculations for three sets of  $A_{rel}$  at fixed parameters  $E^* = 11.0$  MeV and  $E_{flow} = 0.55 \cdot E_{C.M.}$ . The estimated range of  $E^*$  is between the dotted vertical lines.

size of the thermal source with the beam energy is supported by dynamical calculations. For example, the analysis of the FOPI data with the hybrid model  $BUU+SMM$  of ref. [9] has shown that in central Au+Au collisions the fraction of thermalized matter drops from  $A_{rel}=0.48$  at 150 A·MeV to  $A_{rel}=0.3$  at 250 A·MeV, respectively.

**Table 1.** Properties of the thermal sources. Deviations of the parameters given in parentheses are admissible to reproduce the experimental data within the error bars.  $E_{flow}$  is used in the model calculations. The parameters for 100 A·MeV and 1 A·GeV are extrapolated one's.

$E_{beam}$ (A·MeV)	$E^*$ (A·MeV)	$T_{th}$ (MeV)	$A_{rel}$	$E_{flow}$ (A·MeV)
100	$\simeq 9.0$	$\simeq 7.3$	$\simeq 0.81$	10.5(1.5)
150	10.0(1.1)	7.8(0.4)	0.72(0.11)	20.(3.0)
250	10.8(0.8)	8.4(1.1)	0.50(0.05)	32.(6.)
400	15.0(1.4)	11.5(2.4)	0.50(0.13)	56.8(6.)
1050	24.0(2.0)	21.2(5.0)	0.26(0.10)	81.(10.)

**Table 2.** Reproduction of IMF multiplicities.

$E_{beam}$ (A·MeV)	$\langle IMF \rangle$ SMMFC( $4\pi$ )	$\langle IMF \rangle$ data( $4\pi$ )
150	11.61	10.35 $\pm$ 0.06 [13], 12.6 [14]
250	8.42	7.58 $\pm$ 0.04 [13], 8.3 [14]
400	5.50	5.16 $\pm$ 0.03 [13], 5.7 [14]

### 4.3 Radial flow

As start parameter we used results from previous analyses [13, 15, 17, 39] which were slightly varied to get an optimum reproduction of the fragment's mean kinetic energies. The values  $E_{flow}$  and the allowed spread given in table 1 provide a satisfactory agreement between data and calculation. These values are in agreement with other analyses of the data [40].

### 4.4 Energy release by pions

The quantity  $P_\pi$  was estimated (i) from pion multiplicities predicted by Vlassov-Uehling-Uhlenbeck transport model calculations in dependence of the beam energy at impact parameters of  $b=3$  fm [41], (ii) from the  $\Delta$ -resonance production probability in central Au+Au collisions [42], (iii) from the pion-to-proton ratios at 1.05 A·GeV [43] and (iiii) the data in ref. [44]. From all those references one can conclude that pion production at 1.05 A·GeV carries away  $\simeq 10$  % of the available C.M. energy. For the lower considered energies the pion contribution is negligible.

### 4.5 Break-up density

In the model SMM/SMMFC the free volume influencing the translational entropy of partitions is not determined by the total volume (or density) of the system, though this assumption is adopted in some other statistical analyses [14]. The free volume reflects dynamics of fragment formation and it depends on the fragment multiplicity [1]. This ansatz is important for a good reproduction of experimental data [10]. In the model the density influences directly only the Coulomb interaction in the system. The

**Table 3.** Calculated multiplicities of LCP's in central Au+Au collisions using the scenario (ii) and the parameters from table 1. Typical uncertainties in the resulting sum are  $\pm 5$ .

	E(A·MeV)	pre	equ	sum	data [13]
Z=1	150	32.2	32.4	64.6	61.84(0.58)
Z=1	250	52.2	30.8	83.0	75.82(0.62)
Z=1	400	60.0	34.8	94.8	92.04(0.62)
Z=2	150	5.3	15.6	20.9	26.76(0.36)
Z=2	250	8.9	14.5	23.4	27.27(0.36)
Z=2	400	9.3	14.3	23.6	24.16(0.30)

**Table 4.** Same as table 3, but calculations without coalescence.

	E(A·MeV)	pre	equ	sum	data [13]
Z=1	150	40.6	32.4	73.0	61.84(0.58)
Z=1	250	69.0	30.8	99.8	75.82(0.62)
Z=1	400	77.8	34.8	112.6	92.04(0.62)
Z=2	150	1.4	15.6	17.0	26.76(0.36)
Z=2	250	0.6	14.5	15.1	27.27(0.36)
Z=2	400	.1	14.3	14.4	24.16(0.30)

resulting excitation energies of the equilibrated source are large compared to the Coulomb energies so that only minor changes in the fragment yields are expected if the freeze-out density is changed. This was confirmed by corresponding calculations within  $1/6 \leq \rho/\rho_0 \leq 1/3$ , where  $\rho_0$  is the normal nuclear density. Our final calculations were performed with a freeze-out density of  $\rho=1/6 \cdot \rho_0$ .

## 5 Comparison of experimental data with model calculations and discussion

### 5.1 Fragment charge distributions and multiplicities

Since our input parameters for SMMFC have been derived only from the IMF observables it is important to proof to what extent the model reproduces also the LCP multiplicities. Figure 3 and table 2 show that the model is able to reproduce the charge distributions from LCP's to IMF's in shape as well as in absolute scale provided that preequilibrium nucleons and the coalesced particles are taken into account. On the contrary, calculations performed without coalescence show a clear underestimation of the Z=2 multiplicity as seen by comparison of tables 3 and 4 based on the data taken from Ref. [13].

### 5.2 Isotope Temperatures $T_{iso}$

In order to describe the experimental findings shown in Fig. 1 we performed model calculations by using the parameters evaluated in section 4 (see table 1). The calculation at 100 A·MeV was performed with extrapolated pa-



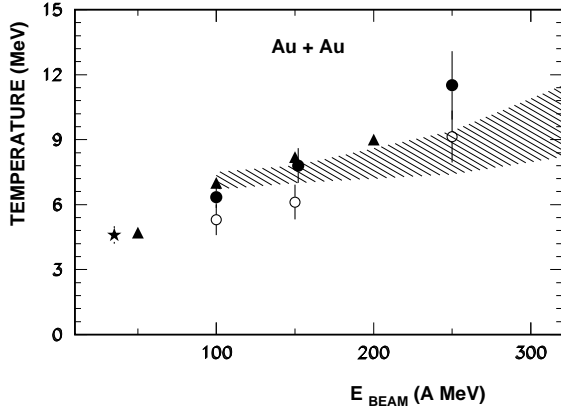


**Fig. 5.** Temperatures as a function of the beam energy. Dots: isotope temperatures obtained from the yield ratios  $d/t$  and  ${}^3\text{He}/{}^4\text{He}$  (integrated over the particles kin. energies)[15,16], open dots: the same but in the velocity range limited by  $v/c \approx 0.3$ , black triangles: the same, taken from [46], black asterisk: temperature from ref. [48], hatched area: limits of the microcanonical temperature calculated with SMMFC using the input parameters of table 1.

rameters given in table 1, which are consistent with parameters extracted in ref. [3]. The generated kinetic energy distributions of  $d, t, {}^3\text{He}$  and  ${}^4\text{He}$  were filtered by the cuts set in the experiment [15]. Then the calculated LCP spectra were transformed into velocity distributions like the experimental data. The temperatures  $T_{H-He}$  obtained from that reproduce almost quantitatively the data (see Fig. 1.)

In the calculations the increase of  $T_{iso}$  with velocity is mainly caused by a combined effect of the thermal and coalescence mechanisms, since they favour production of LCP's with different energies [29]. The temperature in this range of kinetic energies is also sensitive to the radial flow: the simulations undershoot the data if too less radial flow is assumed and overshoot them for too much flow. The parameters within the limits given in table 1 allow a reasonable reproduction of the data.

The isotope temperatures  $T_{iso}$  obtained from energy-integrated yields, as well as from the yields in the limited range of fragment velocities (see section 2) are presented in Fig. 5. This figure shows also results of the ALADIN collaboration obtained for central Au+Au collisions in the energy range from 50 A·MeV to 200 A·MeV [46], as well as data at 35 A·MeV [48], which match also the found trend. Figure 5 shows also the microcanonical temperature  $T_{th}$  of the thermal source calculated with the code SMMFC. As discussed in [45] this temperature is slightly different from  $T_{H-He}$ , however it shows clearly the same behaviour with increasing beam or excitation energy. Therefore, the isotope temperature at low beam energies can be used to deduce the temperature of the thermal source [45].

### 5.3 Kinetic energy spectra

In this section we compare measured kinetic energy distributions of fragments produced at 250 A·MeV and 1 A·GeV with corresponding calculations. Calculations with only the thermal source fail to reproduce the tails of the spectral shapes of  $Z=1$  and  $Z=2$  particles at 250 A·MeV (see Fig. 6). A consideration of the preequilibrium contribution improves the calculated shape. The displayed two data sets of  $Z=1$  distributions demonstrate that the spectral shape is rather sensitive to the criterion how central events are selected. The calculated SMMFC distribution is close to the event sample obtained by the stringent combined criterion of ERAT and directivity (see ref.[13]).

The disagreement of the tails in the proton spectra might be due to deviations of the initial distributions of protons from a one-particle equilibration. Neither the spectral shape nor the multiplicity of light clusters can be reproduced without consideration of coalescence.

Generally, the presence of the radial flow affects the energy spectra and imitates a high temperature. As supposed, the radial velocities of the fragments depend on their positions in the freeze-out volume. This leads to an additional difference between velocities of fragments which is not connected with their thermal random motion. Therefore, the deduced source temperature may be essentially lower than the temperature extracted from fits of kinetic energy distributions to the data. For example, the calculations shown in Fig. 6 were performed with radial flow of  $E_{flow} = 32$  A·MeV. The spectra shapes of lithium clusters generated by a thermal distribution superimposed with this flow are close to the measured data. The Siemens-Rasmussen formula [19], which does not take into account the effect of the fragment positions, reproduces the shape of this distribution also, if the kinetic temperature is  $T_{kin} \simeq 29$  MeV. However, this temperature is considerably larger than the thermal one.

In Fig. 7 we compare the mean kinetic energies calculated also for the heavier clusters with the corresponding data [39]. The satisfactory agreement between data and calculation is consistent with the result of ref. [13] where it was found that  $34.0 \pm 3.9$  A·MeV of the available C.M. energy is stored into the radial flow.

Next we applied SMMFC to analyse data obtained in central Au+Au collisions around 1 A·GeV [16,17]. At this incident energy mostly LCP's are produced and the influence of the thermal source on the fragment production is very limited. The model input parameters  $E^*$  and  $A_{rel}$  (given in table 1) were estimated from the values at low  $E_{beam}$  by straightforward extrapolation. The energy stored in radial flow was taken from ref. [17]. A slight variation of the parameters ( $\pm 12\%$ ) was allowed to find optional agreement with the data. Proceeding on this input, the model calculations<sup>2</sup> give a quite reasonable description of the proton distribution (Fig. 8), demonstrating the

<sup>2</sup> no filter was applied to the calculated events since it was emphasized (ref.[16]) that 'the TPC...allows measurements of spectra up to angles of  $90^\circ$  in the center of mass with *no* low- $p_T$  cut for central events'.

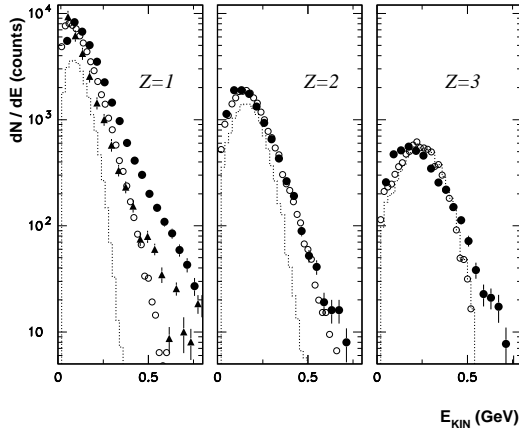


**Fig. 6.** Kinetic energy spectra of ejectiles with charges  $Z=1, 2, 3$  at 250 A-MeV. Full dots: experimental data for the cut  $\Theta_{C.M.} \geq 25^\circ$  and  $ERAT \geq 0.7$ , full triangles: data from ref.[13]. Dashed histogram: thermal spectrum, open circles: sum of thermal and preequilibrium parts (phase space generation, coalescence included). Calculations and data are scaled among themselves to compare the spectral shapes.

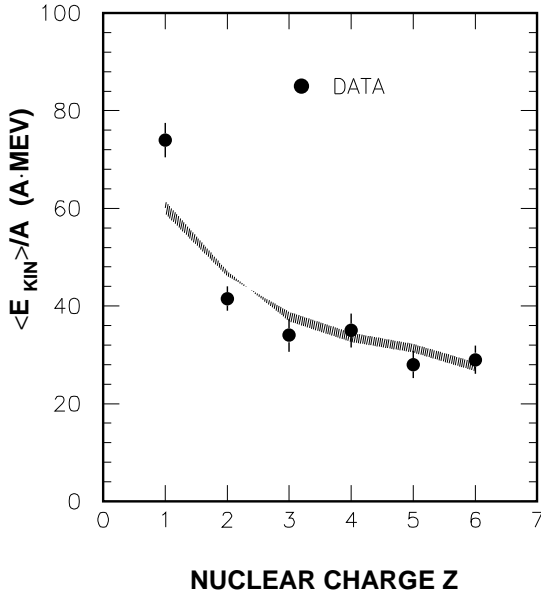


**Fig. 7.** Mean kinetic energies per nucleon at 250 A-MeV. Dots: data from ref. [39] for the azimuthal angle  $\varphi=180^\circ$ . Hatched area : calculations with  $32 \leq E_{flow} \leq 34$  A-MeV.

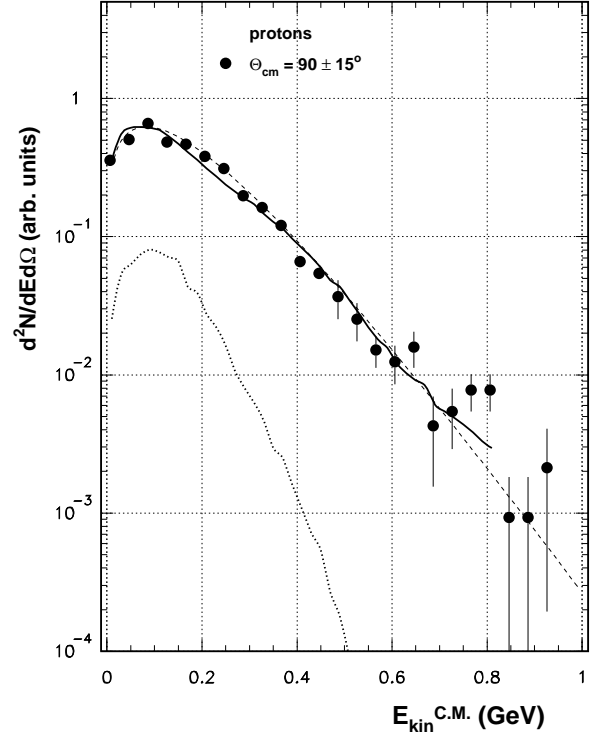


**Fig. 8.** Differential kinetic energy distributions of protons at 1.0 A-GeV. Dots: EOS data [17], dotted line: calculated spectrum of the thermal source, solid line: sum of the fast-stage and thermal sources normalized to the data, dashed line: fit of the calculated proton distribution using the Siemens-Rasmussen relation.

**Table 5.** Multiplicities of LCP's in central Au+Au collisions at 1.0 A-GeV. Upper row: data [16,18], lower row: SMMFC calculations.

protons	deuterons	tritons	$^3\text{He}$	$^4\text{He}$
78.82	33.34	9.56	6.06	2.40
$\pm 1.48$	$\pm 0.98$	$\pm 0.48$	$\pm 0.4$	$\pm 0.26$
84.7	35.9	9.6	9.7	3.6

high degree of one-particle equilibration reached in this central event sample. However, protons from the complete thermalized source contribute only with a very small fraction (see the dotted line in Fig. 8). In tables 5 and 6 we compare experimental and calculated multiplicities and average kinetic energies of LCP's. A sufficient agreement between data and calculations could be achieved. The data given in table 5 were used to calculate the temperature  $T_{H-He} = 18.2 \pm 5.9$  MeV. The corresponding isotope temperature calculated with SMMFC amounts to  $T_{iso} \simeq 18.0$  MeV. However, these temperatures are considerably lower than the kinetic temperatures determined by the slope of the energy spectra.

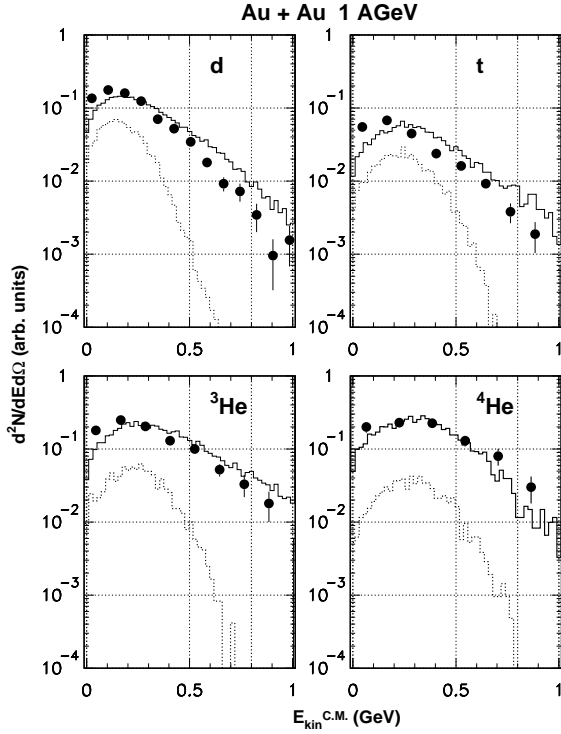


**Fig. 9.** Energy distributions of hydrogen and helium isotopes. Black dots: data taken from ref. [17]. Solid histograms: sum of the fast-stage and thermal sources. Input  $E_{flow} = 90$  A·MeV,  $A_{rel} = 0.26$ ,  $P_{\pi} \simeq 0.10$ . Dashed histograms: the same input, but without coalescence. Calculations are normalized to the data.

**Table 6.** Average kinetic energies  $\langle E_{kin} \rangle$  in central Au+Au collisions at 1.15 A·GeV. Upper row: data [17], lower row: SMMFC calculations.

protons	deuterons	tritons	$^3\text{He}$	$^4\text{He}$
203±3 MeV	263±3 MeV	322±12 MeV	328±12 MeV	359±20 MeV
233±11 MeV	278±18 MeV	331±12 MeV	307±15 MeV	317±15 MeV

In order to illustrate this point we compare our results with the fit of the data performed in [16, 17] based on the blast scenario of Siemens and Rasmussen [19]. In Fig. 8 we show also the corresponding blast model fit to the proton spectrum equivalent to the high kinetic temperature of  $T_{kin} = 81$  MeV [17]. Nearly the same temperature reproduces also the  $d$ ,  $t$ ,  $^3\text{He}$  and  $^4\text{He}$  distributions [17]. The obvious difference between kinetic and isotope temperatures suggests that each of both temperature evaluations is related to different processes.

In Fig. 9. we compare the differential LCP spectra taken from ref. [17] with SMMFC calculations using identical input parameters. A reasonable simultaneous reproduction of the spectral shapes of the above species can be achieved, if coalescence is taken into account. Results

without coalescence (dashed histograms) deliver shapes quite different from the data. The shapes of LCP energy distributions calculated by SMMFC including coalescence are similar to the corresponding one's obtained by the blast-model fits. From that one can conclude that the kinetic temperature, evaluated from such fits, characterizes the initial distribution of nucleons but it is different from the isotope temperature characterizing the chemical composition of the produced fragments.

Using the procedure described in section 2 we obtained the isotope temperature  $T_{H-He}$  as function of the radial velocities. However, contrary to the increasing trend shown in Fig. 1, at 1 A·GeV beam energy the temperature  $T_{H-He}$  does not increase with increasing velocity. Probably, this is a consequence of the coalescence mechanism which is mainly responsible for the LCP production (see also discussion in section 5.4).

#### 5.4 Correlation of the radial flow with the chemical temperature

By comparing Fig. 5 with table 1 one can see that both the isotope temperature, characterizing the produced fragments, and the radial flow, reflecting the dynamics of the process, increase with the beam energy. We suggest that the correlation between these parameters may provide complementary information on mechanisms of fragment production.

As pointed out, there are two contributions to the isotope temperature given by the SMMFC. The first one is related to the fragment production in the thermal source, which dominates at low flow energies. Experimentally, this temperature could be identified approximately at small flow velocities, as seen in Fig. 1. In the following we depict  $T_{H-He}$  extracted at fragment velocities  $v \leq 5$  cm/ns as the 'thermal' isotope temperature. Contrary to this temperature we call isotope temperatures obtained from energy-integrated yields 'total' ones. Figure 10 presents a phenomenological relation between the isotope temperature and the radial flow energy of the thermal sources. The 'thermal' isotope temperatures, shown in Fig. 10 as open circles, increase with increasing radial flow. With regard to other experimental data we note that the isotope temperature corresponding to central Au on Au collisions at 35 A·MeV [48] should be considered also as the 'thermal' one, since the dominating thermal source includes the small radial flow energy of  $\leq 1$  A·MeV[2].

The second contribution to the isotope temperature comes from the coalescence mechanism and it provides higher values of the temperature. In order to compare both contributions, we show in Fig. 10 the total isotope temperatures obtained from the same data. In addition, we included into this figure also 'total' isotope temperatures  $T_{H-He}$  obtained in central Au+Au collisions at 50, 100, 150 and 200 A·MeV taken from ref. [46]. The corresponding radial flow energies were estimated by interpolation of the values given in table 1 and they are close to other results [3, 9, 40].

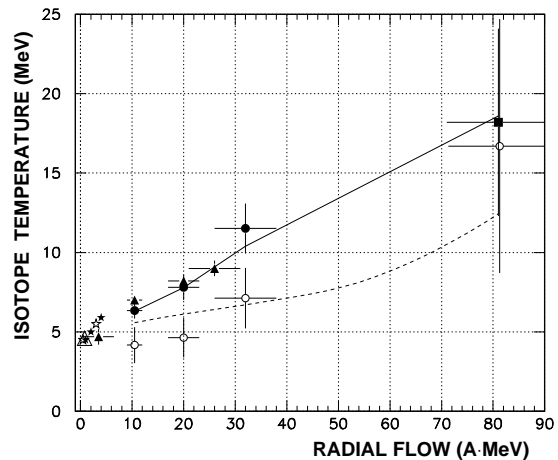
The found difference between the 'total' and 'thermal' isotope temperatures indicates the existence of the two contributions. At small flow energies the difference increases with increasing flow, because the contribution of the coalescence becomes larger. This difference is supposed to decrease at large flow energies, since the contribution of the completely thermalized source disappears. At 1 A-GeV beam energy, IMF are scarcely produced. Therefore, there are large uncertainties in both the radial flow and the isotope temperature contributions obtained for the thermal source. However, within the error bars no difference between the 'total' and the 'thermal' chemical temperatures was found. That is consistent with the disappearance of the thermalized source. The comparison of the 'thermal' and the 'total' temperatures shown in Fig. 10 suggests that the transition between the described mechanisms accomplishes rather smoothly since the temperatures are not very different.

Figure 10 shows also data obtained from another type of reactions, namely break-ups of Au nuclei after peripheral collisions [10, 11]. These data correspond to small flow energies and they match the general trend indicating that the fragment formation seems to correlate with the appearance of the radial flow independently of its origin.

From the obtained results we suggest the following evolution of the fragment production process with increasing radial flow. As long as the flow is small, the fragments are mainly produced in a completely equilibrated source. However, the energy available for the thermal population of the phase space does not include the flow energy. Increasing radial flow influences the fragment formation in a twofold way: (i) it increases the velocities of nucleons forming a fragment, and (ii) it restricts the phase space population by cutting many-particle correlations between nucleons. This leads to the production of small fragments, which could be effectively described as increasing temperature of the thermal source. At larger radial flow, only one-particle correlations remain, which correspond to the coalescence mechanism. Nevertheless, properties of composite particles produced by coalescence resemble features of statistical processes. In particular, one may introduce a *common* temperature for any of the fragments which characterizes their formation probabilities and which is an ingredient of the chemical equilibrium. Therefore, one can formally proceed to treat the fragment formation statistically, but taking into account the specific relations between the new 'statistical' parameters caused by the dynamics of the process (see, e.g., relation (13)). Some relations of the standard thermodynamics, such as the equivalence of the chemical and the kinetic temperatures, are not valid in this case. However, one can deduce relations between statistical and dynamical parameters, like that shown in Fig. 10.

## 6 Conclusions

We have developed an extended version of the Statistical Multifragmentation Model (SMMFC) aimed at the analysis of experimental data related to LCP and IMF produc-



**Fig. 10.** Isotope temperatures versus radial flow. Open circles: thermal temperatures estimated at low fragment velocities. Open triangle: thermal temperature taken from [48]. Full symbols correspond to temperatures obtained from energy-integrated isotope yields. Dots: FOPI data [15]. Triangles: ALADIN data [46]. Square: EOS data [16, 17]. Full asterisks: peripheral collisions from [10]. Open asterisks: peripheral collisions from [11, 47]. Dashed line: Calculated isotope temperature of the thermal source alone. Solid line: isotope temperature  $T_{H-He}$  calculated by SMMFC including coalescence.

tion in central heavy-ion collisions. In the present studies the model was applied to analyse Au+Au data obtained by the FOPI and EOS collaborations in the energy range from 100 to 400 and at 1000 A-MeV, respectively.

The statistical analysis includes the following physical processes of the reactions. An essential part of nucleons of the whole system is released during the fast (dynamical) stage and the remaining matter constitutes an equilibrium source. The share of the complete thermalized source  $A_{rel}$  decreases with increasing beam energy. This result is in agreement with analyses of experimental data carried out in refs. [3, 5, 9]. It was found that the thermal sources have temperatures which are considerably lower than expected from the kinetic energies of the produced fragments. Both the nucleon and the LCP emissions in the fast stage are supposed to be the reason of the reduced equilibrated energy at the freeze-out. Moreover, an appreciable part of the available energy of the equilibrated source is converted into collective motion, e.g. radial flow. Though the analysis remains phenomenologically in part, the found regularities seem to be reliable since they are supported also by analyses of other data. Therefore, the results may be used for interpolation and qualitative estimations of parameters of thermal sources.

According to our findings, a considerable growth of the flow energy is accompanied by a very moderate increasing of the thermal temperature in these central collisions. In our opinion, the most reliable determination of the temperature in this case should be achieved by the isotope

thermometer which can be directly related to the thermal source. As we have shown, it is possible to apply this thermometer for testing the dependence of the temperature on the fragment velocities, which can be used to identify different mechanisms of fragment production.

Light clusters can also occur as result of a dynamical process which involves secondary interaction of the fast nucleons. We have shown that the coalescence mechanism is responsible for the production of light fragments and its contribution dominates at larger beam energies. Coalescence is caused by the short range attractive interaction between the nucleons, and, under some conditions, it is consistent with the chemical equilibrium. Nevertheless, the isotope temperatures obtained from yields of coalescent fragments remain very moderate in comparison with their kinetic energies (i.e. with their kinetic temperatures). The analysis of experimental LCP energy distributions leads also to this conclusion. Therefore, one can speculate that the chemical equilibrium is attained in such exploding systems. However, it is different from the one-particle kinetic equilibration. We have demonstrated that the isotope temperature is correlated to the radial flow in central collisions. This presumed relation between isotope temperature and radial flow may be used to estimate chemical temperatures in different explosive processes.

*Acknowledgements* W.N. thanks for a long collaboration within the FOPI project, A.S.B. thanks the GSI Darmstadt for hospitality and financial support. The authors thank especially Dr. W. Reisdorf for numerous stimulating discussions and Dr. H.W. Barz for valuable comments. We are also indebted to Drs. H. Prade and F. Dönau for a careful reading of the manuscript.

## References

- J.P. Bondorf, A.S. Botvina, A.S. Iljinov, I.N. Mishustin and K. Sneppen, Phys. Rep. **257**, 133 (1995)
- M. D'Agostino et al., Phys. Letters B **371**, 175 (1996)
- F. Lavaud, Ph.D. thesis, IPNO T 01-06, IPN Orsay, 2001, unpublished
- B. Borquet et al., *Proceedings of the 39. International Winter Meeting on Nuclear Physics, Bormio, 2001* edited by I.Iori and A.Moroni (Supplement 117, University of Milano, 2001), p. 84-102
- C. Williams et al., Phys. Rev. C **55**, R2132 (1997)
- W. Neubert FOPI Collaboration, *Proceedings of the International Workshop on Heavy Ion Physics at Low, Intermediate and High Energies using 4 $\pi$  detectors, Poiana Brasov (Romania), 1996*, edited by M.Petrovici et al. (World Scientific, Singapore 1997), p. 194 and private communication
- J.P. Bondorf et al., Phys. Rev. Lett. **73**, 628 (1994)
- P. Dessesquelles et al., Nucl. Phys. A **633**, 547 (1998)
- B. Heide and H.W. Barz, Nucl. Phys. A **588**, 918 (1995) and Nucl. Phys. A **591**, 755 (1995)
- R.P. Scharenberg et al., Phys. Rev. C **64**, 054602 (2001)
- H. Xi et al., Z. Phys. A **359**, 397 (1997)
- G. Wallerstein et al., Rev. Mod. Phys. **69**, 995 (1997)
- W. Reisdorf et al., FOPI collaboration, Nucl. Phys. A **612**, 493 (1997) and Acta Phys. Polonia C **52**, 443 (1994)
- C. Kuhn et al., FOPI collaboration, Phys. Rev. C **48**, 1232 (1993)
- G. Poggi et al., FOPI collaboration, Nucl. Phys. A **586**, 755 (1993)
- M.A. Lisa, EOS Collaboration, *Proceedings of the International Workshop on Heavy Ion Physics at Low, Intermediate and High Energies using 4 $\pi$  detectors, Poiana Brasov (Romania), 1996*, edited by M.Petrovici et al. (World Scientific, Singapore 1997), p. 194 and private communication
- M.A. Lisa et al., EOS collaboration, Phys. Rev. Lett. **75**, 2662 (1995)
- A. Scott, Ph.D. thesis, Kent State University, 1995, unpublished
- P.J. Siemens and J.O. Rasmussen, Phys. Rev. Lett. **42**, 880 (1979)
- D. Hahn and H. Stöcker, Nucl. Phys. A **476**, 718 (1988)
- G. Fai and J. Randrup, Comp. Phys. Comm. **42**, 385 (1986) and Comp. Phys. Comm. **77**, 153 (1993)
- A.S. Botvina et al., Nucl. Phys. A **475**, 663 (1987)
- S. Albergo et al., Il Nuovo Cimento **89**, 1 (1985)
- T. Möhlenkamp, Ph.D. thesis, Technische Universität Dresden, 1996, unpublished
- J. Pochodzalla et al., Phys. Rev. Lett. **75**, 1040 (1995)
- G.I. Kopylov, *Principles of resonance kinematics*, ( Nauka, Moscow, 1970)
- H. Xi et al., Phys. Rev. C **57**, R462 (1998)
- K.G.R. Doss et al., Phys. Rev. Lett. **59**, 2720 (1987) and Mod. Phys. Lett. A **3**, 849 (1988)
- W. Neubert and A.S. Botvina, Eur. Phys. J. A **7**, 101 (2000)
- S.T. Butler and C.A. Person, Phys. Rev. **129**, 836 (1963)
- H.H. Gutbrod et al., Phys. Rev. Lett. **37**, 667 (1976)
- L.P. Csernai and J.I. Kapusta, Phys. Rep. **131**, 223 (1986)
- D.H.E. Gross, Rep. Progr. Phys. **53**, 605 (1990)
- E. Fermi, Prog. Theor. Phys. **5**, 570 (1950)
- A. Mekjian, Phys. Rev. Lett. **38**, 640 (1977)
- J. Cibor et al., Phys. Lett. B **473**, 29 (2000)
- J.B. Bondorf et al., Nucl. Phys. A **624**, 706 (1997)
- C.B. Das and S. Das Gupta, Phys. Rev. C **64**, 041601 (2001) and F. Gulminelli and Ph. Chomaz, **nucl-th/0209032**, 2002
- M. Petrovici et al., FOPI collaboration, Phys. Rev. Lett. **74**, 5001 (1995)
- W. Reisdorf and H.G. Ritter Annu. Rev. Part. Sci. **47**, 663 (1997)
- H. Stöcker and W. Greiner, Phys. Reports **137**, 277 (1986)
- R. Averbeck et al., GSI-Nachrichten 10-95, 1995, unpublished
- D. Pelte, FOPI collaboration, Z. Phys. A **359**, 55 (1997) and Z. Phys. A **357**, 215 (1997)
- C. Müntz et al., Z. Phys. A **357**, 39 (1997)
- J.B. Bondorf et al., Phys. Rev. C **58**, R27 (1998)
- V. Serfling et al., ALADIN collaboration, Phys. Rev. Lett. **80**, 3928 (1998)
- T. Odeh, Ph.D. thesis 99-15, University of Frankfurt am Main, 1999, unpublished
- M.J. Huang et al., Phys. Rev. Lett. **78**, 1648 (1997)